Comput Geosci (2012) 16:277–296
DOI 10.1007/s10596-011-9267-x

ORIGINAL PAPER

A model for conductive faults with non-matching grids

Xavier Tunc · Isabelle Faille · Thierry Gallouët · Marie Christine Cacas · Pascal Havé

Received: 31 January 2011 / Accepted: 8 November 2011 / Published online: 9 December 2011

Abstract In this paper, we are interested in modeling single-phase flow in a porous medium with known faults seen as interfaces. We mainly focus on how to handle non-matching grids problems arising from rock displacement along the fault. We describe a model that can be extended to multi-phase flow where faults are treated as interfaces. The model is validated in an academic framework and is then extended to 3D non K-orthogonal grids, and a realistic case is presented.

Keywords Porous media · Faults · Interface model · Non-matching grids · Finite volume

Mathematics Subject Classifications (2010) 76S05 · 35Q86

X. Tunc (✉) · I. Faille · M. C. Cacas · P. Havé
IFP Energies nouvelles, 1-4 avenue de Bois-Préau,
92852 Rueil-Malmaison Cedex, France
e-mail: xavier.tunc@gmail.com

I. Faille
e-mail: isabelle.faille@ifpen.fr

M. C. Cacas
e-mail: marie-christine.cacas-stenz@ifpen.fr

P. Havé
e-mail: pascal.have@ifpen.fr

T. Gallouët
LATP, CMI, 39 rue Frédéric Joliot-Curie,
13453 Marseille Cedex 13, France
e-mail: gallouet@cmi.univ-mrs.fr

1 Introduction

The importance of fractures in hydrocarbon exploration and exploitation has already been demonstrated and investigated. Since the early 1960s, a large number of studies has been performed, to take into account their influence on fluid flow. The faults can be characterized as extended fractures, across which there has been a relative displacement of rocks on either side. Faults are rarely only geometrical discontinuities but rather zones of deformed rocks with particular fluid flow properties. Fault zones have a small width compared to basin or reservoir scale, and due to fracturation and possible reactions, their properties can be very different from the surrounding host rock. They are assimilated to a porous media and could act as a barrier or a conduit for fluid migration. Therefore, it becomes necessary to model the fluid flow along the faults and to integrate them in reservoir, basin and CO_2 storage simulations. Several difficulties are encountered when modeling fluid flows along the faults. Firstly, the heterogeneous nature of the fault–matrix system leads to very different space and time scales between matrix and fault flow. Then, fault throw is usually accounted for through non-matching grids across which there can be large jumps in flow properties. Finally, faults are rarely isolated planar objects but rather non-planar surfaces organized in complex networks.

In reservoir simulation, faults are commonly handled through fluxes across the non-matching interfaces that use fault transmissibility multipliers [19]. These fault transmissibility multipliers are generally calculated based on fault properties estimates (permeability and width) that can be evaluated via the Shale Gouge Ratio and the throw [24]. To account for fluid flow

along the fault zones, several models have already been proposed. Trocchio [23] and Gilman et al. [15] tried unsuccessfully to homogenize the permeability of the fault with the neighboring matrix blocks. They concluded that the faults must be modeled explicitly. This approach was followed by [16] and [15], who used volumetric small cells with high permeabilities to represent the faults. In the same framework of volumetric modeling, [13] proposed an approach for building and populating the fault zone grid that accounts for its 3D architecture. Although accurate, volumetric fault modeling is computationally expensive and requires appropriate mesh builders.

Thanks to the difference of scales between reservoirs or basins and faults, a fault can be considered, on a geometrical point of view, as an interface between two blocks of rock, the fault width then becoming a model parameter. This approach leads to the so-called interface model. Lee et al. [18] followed a well-like approach, where the potential distribution is supposed to be at the hydrodynamic equilibrium. The fault volume is neglected in this model and therefore cannot take into account the distribution of several fluids inside the fault. Faille et al. [9], Martin et al. [20] and Angot et al. [5] derived an interface model from the volumetric one, to simulate a single-phase flow along the fault for matching grids. In this model, the equations for the matrix subdomains remain unchanged whereas the flow inside the $(n-1)$-dimensional fault is obtained by averaging the previous equations across the width of the fault. Part of this model has been described in [2–4, 6, 11, 12]. The model they propose is easily extendable to multi-phase flow. Reinchenberger et al. [22] proposed a similar model but only for permeable faults. Karimi-Fard et al. [17] studied the case of fracture networks for multi-phase flow and used a parallel between fault networks and electric resistances, to calculate equivalent transmissivities. Finally, [14] applied this model for a single-phase flow ruled by the Forcheimer's law. The authors treat non-matching meshes in their paper but only for permeable faults, across which the pressure is continuous. To our knowledge, there are no results with non-matching grids for both permeable and impermeable faults.

This work intends to propose a model for fluid flow along faults that could be integrated into standard oil industry fluid flow simulators. So it has to be usable for standard corner point geometry (CPG [21], see Fig. 1) grids where the faults are represented by surfaces across which the grid is non-matching. Even though only single-phase flow is considered in the framework of this paper, the approach retained must be easily extendable to multi-phase flow. This work follows the approach of [5, 9, 20] and is based on an interface representation of the fault zone that addresses the problem of space scales.

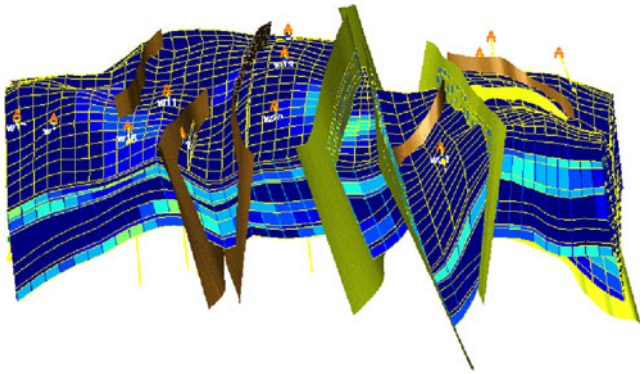

Fig. 1 Example of CPG mesh

In order to handle non-matching grids, several possibilities exist to represent the faults. The most intuitive one would be to use a common refined grid of the two fault surfaces. However, considering the complex geometry involved, eventually including fault networks, this seems hardly applicable in 3D. Another possibility would be to use one-single independant interface to represent the fault. This method could lead to good results but adds a major difficulty. Indeed, two non-matching exchanges terms should be computed with the neighbouring matrix. Besides the drawbacks pointed out, these two methods to represent faults require to introduce additional grid elements. One approach to avoid the modelization difficulties previously listed would be to use a single interface coming from the reservoir grid. Nevertheless, this method requires to choose one of the two non-matching surfaces and therefore gives artificially a preferential role to one side of the fault. Finally, we choose to represent the fault with the two non-matching interfaces, each side of the fault being meshed conformal with its neighbouring matrix block. This representation does not require to introduce additional grid elements, implies only one non-matching exchange terms, between the two sides of the fault, and gives the same importance to the two non-matching interfaces.

Moreover, the difficulty then associated to the non-matching grids can be compared to the one classically handled when considering only flow across faults. This approach uses different meshes on either side of the fault, respecting therefore the geological layering. In the discretised equations, the non-matching fault cells are connected through "fault–fault" flux terms across the two parts of the fault. This approach can be naturally combined with standard cell-centered finite

volume discretisation and could therefore be extended to multi-phase flow.

In the first part of this paper, we consider a model problem that allows us to investigate how the non-matching grids can be handled. Namely, we restrict ourselves to a single linear fault that connects two rectangular subdomains, each of them being meshed independently with a cartesian grid. The first section is dedicated to the obtention and presentation of the interface fault model. Then, a finite volume discretisation is introduced. Results obtained on non-matching grids, for permeable, impermeable and anisotropic faults, in homogeneous or heterogeneous media are then exposed and compared to a co-refined reference solution.

The second part of the paper is a step forward towards real case simulation. Still considering single-phase flow, we extend the discretised model to more general grids such as CPG or unstructured grids. Some numerical results illustrate the ability of the proposed approach to account for flow along faults.

2 A simple model problem

In this first part, we want to study how the proposed approach behaves with grids that are non-matching across the faults. In order to focus on this particular point, we deal with a model problem for which the non-matching characteristic of the grid is the main difficulty.

Indeed, restricting ourselves to a 2D framework, we consider a single 1D linear vertical fault that cuts a domain into two subdomains independently meshed with cartesian grids (see Fig. 2). This 1D linear discretisation of the fault zone aims at representing a volumetric fault zone that is very thin compared to the domain size. The true volumetric description of the fault zone will be used as a reference domain where a reference solution can be computed and with which the proposed model can be compared.

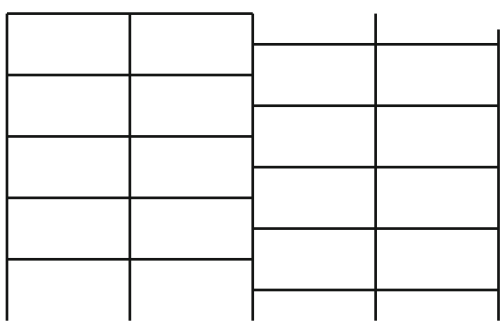

Fig. 2 1D linear vertical fault

In the following, we first introduce the interface fault model in a continuous framework. This model is derived from the volumetric model, assuming that the fault width is small compared to the domain size. Then, we propose a cell-centered finite volume discretisation which, compared to the standard discretisation without faults, adds several exchange terms namely fault–matrix, along fault fluxes and across fault fluxes which take into account the non-matching interface. In the finite elements or mixed finite elements framework, this problem is usually treated with mortar and domain decomposition methods [7]. In the finite volume framework, this approach was studied in [10] where the authors showed that in a highly heterogeneous media, it leads to poor results. We therefore consider here directly finite volume fluxes discretisations on non-matching grids. The accuracy of the proposed discretised model is finally studied numerically for different assumptions on the fault properties.

2.1 Derivation of the interface model

Considering incompressible single-phase flow in porous media and neglecting gravity, we first describe the volumetric model that governs fluid flow in a domain of rectangular shape cut by one single vertical fault subdomain of small width. We then derive the interface model where the rectangular fault subdomain is replaced by two vertical interfaces, using the technique of averaging across the fault. Compared with previous works [5, 9, 20], the main difference in the proposed approach consists in distinguishing the two sides of the fault and therefore in averaging over each half of the volumetric fault subdomain instead of averaging over the whole fault width. Let us consider a convex domain Ω in $\mathbb{R}^2$, composed of three subdomains: two matrix domains Ω_1 and Ω_2 separated by one single fault domain Ω_f of width b_f, defined by:

$$\Omega_f = \left\{ s + r\mathbf{n};\ s \in \Sigma, r \in \left]-\frac{b_f}{2}, \frac{b_f}{2}\right[\right\}$$

where Σ is a 1D line segment, $\mathbf{t}$ its unit tangent and $\mathbf{n}$ its unit normal. For the sake of simplicity, we assumed that the normal $\mathbf{n}$ is always oriented from Ω_1 to Ω_2. We denote by Γ_i the boundaries of the domain Ω_i, $i = 1, 2$, f and by Σ_i the common boundaries between Ω_i and Ω_f, $i = 1, 2$. Finally, $\partial\Sigma$ denotes the boundaries of Σ.

Figure 3 shows the volumetric and the interface representations of the faulted domain and the considered notations.

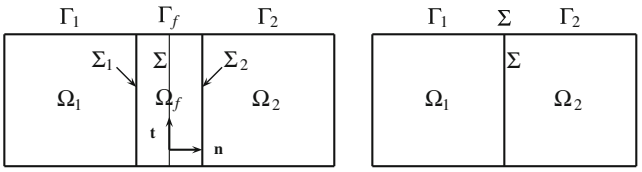

Fig. 3 Faulted domain. *Left* volumetric representation. *Right* interface representation

2.1.1 Volumetric model

Incompressible single-phase fluid flow in the porous domain Ω is governed by mass balance coupled with Darcy's law. The fault zone appears only as a part of the domain with specific fluid flow properties (permeability). However, to simplify the interface model derivation, the volumetric model is directly decomposed into a set of three problems, one for each subdomain, linked together through transmission conditions.

Mass balance equation in each subdomain Ω_i, $i = 1, 2, f$, writes:

$$\nabla \cdot \mathbf{v_i} = q_i \quad \text{in } \Omega_i \tag{1}$$

where $\mathbf{v_i}$ is Darcy's velocity and q_i the source term in domain Ω_i.

Darcy's law is given by, for $i = 1, 2, f$:

$$\mathbf{v_i} = -\mathbf{K_i}\nabla p_i \quad \text{in } \Omega_i \tag{2}$$

where $\mathbf{K_i}$ is the permeability tensor, which is considered diagonal, and p_i the pressure in the subdomain Ω_i, $i = 1, 2, f$. Fluid viscosity is assumed to be equal to 1.

The transmission conditions between the subdomains express flux and pressure continuity across subdomains interfaces:

$$p_i = p_f \quad \text{on } \Sigma_i, \quad i = 1, 2 \tag{3}$$

$$\mathbf{v_i}.\mathbf{n} = \mathbf{v_f}.\mathbf{n} \quad \text{on } \Sigma_i, \quad i = 1, 2 \tag{4}$$

Finally, we consider the following Dirichlet boundary conditions, for $i = 1, 2, f$:

$$p_i = p_i^D \quad \text{on } \Gamma_i, \tag{5}$$

where Γ_i denotes the external boundaries of Ω_i, $i = 1, 2, f$ and p_i^D the imposed pressure. So, the volumetric model consists in the Eqs. 1–5.

2.1.2 Interface model

In the interface model, we reduce the volumetric representation of the fault subdomain Ω_f to its interface representation Σ. To do so, let us start by decomposing Darcy's velocity in the fault domain following its normal and tangential components: $\mathbf{v_f} = \mathbf{v_{f,n}} + \mathbf{v_{f,t}}$, where $v_{f,n} = (v_{f.n})n$ and $v_{f,t} = (v_f.t)t$.

From the volumetric unknowns, we keep (Fig. 4):

- The trace on each side of the fault of:
  - The normal component of the fault velocity: $v_{fn,1}$ on Σ_1 and $v_{fn,2}$ on Σ_2
  - The pressure: $p_{f,1}$ on Σ_1 and $p_{f,2}$ on Σ_2.
- The mean across each half of the fault of:
  - The along component of the fluxes: $\mathbf{V_{f,I}} = \int_{-b_{f/2}}^{0} v_{f,t}\mathrm{d}r$, $\mathbf{V_{f,II}} = \int_{0}^{b_{f/2}} v_{f,t}\mathrm{d}r$
  - The pressure: $P_{f,\mathrm{I}} = \frac{2}{b_f}\int_{-b_{f/2}}^{0} p_f \mathrm{d}r$ and $P_{f,\mathrm{II}} = \frac{2}{b_f}\int_{0}^{b_{f/2}} p_f \mathrm{d}r$
- The trace of the normal component of the fault velocity $v_{fn,\mathrm{I/II}}$ on the central segment Σ

To obtain the interface model, we average the mass balance equation across each half of the fault. We get two averaged mass balance equations that rule the fluid flow along the fault. These equations are coupled with the matrix through a fault–matrix flow obtained by performing two Taylor expansions, one for each side of the fault. They are also linked through a fault–fault flow, obtained thanks to another Taylor expansion.

Let us start by rewriting the mass balance equation inside the fault as:

$$\nabla_{\mathbf{n}} \cdot \mathbf{v_f} + \nabla_{\mathbf{t}} \cdot \mathbf{v_f} = q_f \quad \text{in } \Omega_f \tag{6}$$

where $\nabla_{\mathbf{n}}\cdot$ and $\nabla_{\mathbf{t}}\cdot$ are, respectively, the normal and tangential divergence.

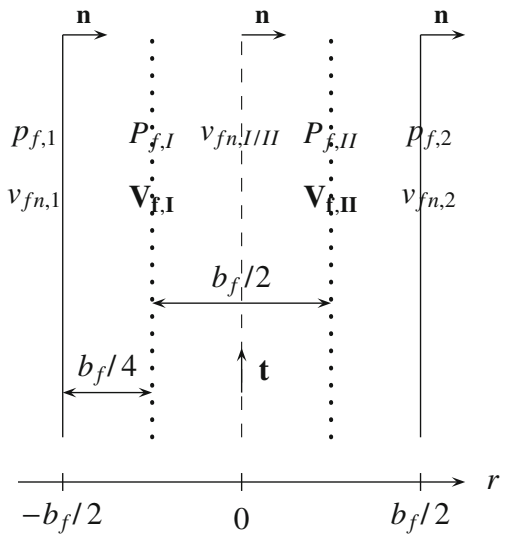

Fig. 4 From volumetric to interface unknowns

We present the derivation of the model only for one side of the fault ($[-b_f/2, 0]$), the equations for the other side of the fault are obtained in a similar way.

Integrating the mass conservation Eq. 6 across $[-b_f/2, 0]$, one obtains:

$$v_{fn,\mathrm{I/II}} - v_{fn,1} + \nabla_{\mathbf{t}} \cdot \mathbf{V}_{\mathbf{f},\mathrm{I}} = Q_{f,\mathrm{I}} \quad \text{on } \Sigma$$

where $Q_{f,\mathrm{I}} = \int_{-b_f/2}^{0} q_f \mathrm{d}r$.

This equation is the conservation equation on the fault interface Σ linked to the other side of the fault through the fault–fault exchange term $v_{fn,\mathrm{I/II}}$ and linked to the neighbouring matrix domain equations through the matrix–fault exchange term $v_{fn,1}$.

Darcy's law can also be decomposed into a normal and tangential component:

$$\mathbf{v}_{\mathbf{f},\mathbf{t}} = -K_{ft} \nabla_{\mathbf{t}} p_f \text{ in } \Omega_f \tag{7}$$

$$\mathbf{v}_{\mathbf{f},\mathbf{n}} = -K_{fn} \nabla_{\mathbf{n}} p_f \text{ in } \Omega_f \tag{8}$$

where $\nabla_{\mathbf{n}}$ and $\nabla_{\mathbf{t}}$ represent, respectively, the normal and tangential gradient and K_{ft} and K_{fn} the normal and tangential component of the permeability.

Averaging Eq. 7 across the half of the fault, one obtains:

$$\mathbf{V}_{\mathbf{f},\mathrm{I}} = -K_{ft} \frac{b_f}{2} \nabla_{\mathbf{t}} P_{f,\mathrm{I}} \text{ on } \Sigma$$

This equation can be seen as Darcy's law along one side of the fault interface.

The boundary condition is:

$$P_{f,\mathrm{I}} = P^D_{f,\mathrm{I}} \text{ on } \partial\Sigma,$$

where $P^D_{f,\mathrm{I}} = \frac{2}{b_f} \int_{-b_f/2}^{0} p^D_f \mathrm{d}r$.

Equation 8 has not yet been introduced in our reduced model. We replace it by performing a first-order Taylor expansion across the first quarter of the fault $[-b_f/2, -b_f/4]$ the width being very small; one obtains:

$$v_{fn,1} = -\frac{4K_{fn}}{b_f}(P_{f,\mathrm{I}} - p_{f,1}) \tag{9}$$

The equations for the other side of the fault are obtained in a similar way. The last equation, coupling the equations along the two sides of the fault, is obtained by performing another first-order Taylor expansion across the half fault width ($[-b_{f/4}, b_{f/4}]$):

$$v_{fn,\mathrm{I/II}} = -\frac{2K_{fn}}{b_f}(P_{f,\mathrm{II}} - P_{f,\mathrm{I}}) \tag{10}$$

The interface model is finally completed by the transmission conditions with the matrix subdomains (Eqs. 3 and 4) that write with the considered fault unknowns:

$$p_{f,1} = p_{1_{|\Sigma}}, \quad v_{fn,1} = \mathbf{v_1}.\mathbf{n}_{|\Sigma}, \quad \text{on } \Sigma$$

where $\mathbf{v_1}.\mathbf{n}_{|\Sigma}$ denotes the trace of $\mathbf{v_1}.\mathbf{n}$ on Σ.

In [20], one can find other relations for Eq. 9, obtained using different quadrature formulas to link the flow and the unknowns on the interfaces. It is possible to sum up the different possibilities using two parametrised equations. The equations we use here are equivalent to the parametrised ones, taking a particular value of this parameter.

Finally, the complete interface model is:

$$v_{fn,\mathrm{I/II}} - v_{fn,1} + \nabla_{\mathbf{t}} \cdot \mathbf{V}_{\mathbf{f},\mathrm{I}} = Q_{f,\mathrm{I}}, \quad \text{on } \Sigma \tag{11}$$

$$-v_{fn,\mathrm{I/II}} + v_{fn,2} + \nabla_{\mathbf{t}} \cdot \mathbf{V}_{\mathbf{f},\mathrm{II}} = Q_{f,\mathrm{II}}, \quad \text{on } \Sigma \tag{12}$$

$$\mathbf{V}_{\mathbf{f},\mathrm{I}} = -K_{ft} \frac{b_f}{2} \nabla_{\mathbf{t}} P_{f,\mathrm{I}}, \quad \text{on } \Sigma \tag{13}$$

$$\mathbf{V}_{\mathbf{f},\mathrm{II}} = -K_{ft} \frac{b_f}{2} \nabla_{\mathbf{t}} P_{f,\mathrm{II}}, \quad \text{on } \Sigma \tag{14}$$

$$v_{fn,1} = -\frac{4K_{fn}}{b_f}(P_{f,\mathrm{I}} - p_{f,1}), \text{ on } \Sigma \tag{15}$$

$$v_{fn,2} = -\frac{4K_{fn}}{b_f}(p_{f,2} - P_{f,\mathrm{II}}), \quad \text{on } \Sigma \tag{16}$$

$$v_{fn,\mathrm{I/II}} = -\frac{2K_{fn}}{b_f}(P_{f,\mathrm{II}} - P_{f,\mathrm{I}}), \text{ on } \Sigma \tag{17}$$

$$P_{f,j} = P^D_{f,j}, \quad \text{on } \partial\Sigma, \quad j = \mathrm{I}, \mathrm{II} \tag{18}$$

$$p_{f,i} = p_{i_{|\Sigma}}, \quad v_{fn,i} = \mathbf{v_i}.\mathbf{n}_{|\Sigma}, \text{ on } \Sigma, \quad i = 1, 2 \tag{19}$$

2.1.3 Discretisation of the interface model

In order to focus on the difficulties associated to the interface fault model and particularly to the non-matching grids across the fault, we consider only matrix subdomains meshed with cartesian grids. Most of the notations used here are largely inspired by [6] and [8]. The interface model is discretised using a cell-centered finite volume scheme, with a two-point flux approximation where orthogonality properties are satisfied. Let $\Omega_{i,h}$ be a cartesian mesh of Ω_i, $i = 1, 2$.

As the mesh is defined independently in each subdomain, the interface Σ is represented by two different 1D meshes, one for each subdomain. Once again we take advantage of the symmetry of the model and describe only one part of the discretisation. Let us denote by $\Sigma_{\mathrm{I},h}$ the set of edges of the mesh of $\Omega_{1,h}$ that are in Σ. The idea is to discretise each mass balance equation along the fault on the more appropriate mesh that is to say Eq. 11 on $\Sigma_{\mathrm{I},h}$ as it has an exchange term with Ω_1 via

the transmission conditions. We will denote by κ or $\mathcal{L}$ a cell of $\Omega_{1,h}$ and by σ or γ an edge of $\Sigma_{\mathrm{I},h}$.

Finally, $m(\sigma)$ denotes the measure of the edge σ, $d_{\sigma,\sigma'}$ the distance between the centers of the edges σ and σ', $d_{\mathcal{K}(\sigma),\sigma}$ the distance between the center of cell κ and the center of edge σ, σ being an edge of κ. Figure 5 presents the notations used for all elements in the mesh.

We introduce the following discrete unknowns:

- For each cell κ of $\Omega_{1,h} \cup \Omega_{2,h}$, $p_{\mathcal{K}}$ the pressure at the cell center
- For each edge σ of $\Sigma_{\mathrm{I},h}$ (resp. $\Sigma_{\mathrm{II},h}$):
  - p^1_σ (resp. p^2_σ) the approximation of p_1 (resp. p_2) at the edge center
  - P^f_σ the approximation of $P_{f,\mathrm{I}}$ (resp. $P_{f,\mathrm{II}}$) at the edge center
  - $p^{f,1}_\sigma$ (resp. $p^{f,2}_\sigma$) the approximation of $p_{f,1}$ (resp. $p_{f,2}$) at the edge center

Flow in the matrix The finite volume scheme in the matrix is the same as the one for the volumetric case.

$$\sum_{\substack{\delta,\\ \delta \text{ edge of } \mathcal{K}}} F_{\mathcal{K},\delta} = m(\kappa) Q_{1,\mathcal{K}}, \quad \forall \mathcal{K} \in \Omega_{1,h} \tag{20}$$

where $Q_{1,\mathcal{K}} = \frac{1}{m(\mathcal{K})} \int_{\mathcal{K}} Q_1 \mathrm{d}s$.

The flux $F_{\mathcal{K},\delta}$ approximates $\int_\delta \mathbf{v_1}.\mathbf{n}_{\mathcal{K},\delta}$ across the edge δ, out of κ. For $\delta = \kappa|\mathcal{L}$, flux conservation and continuity of the pressure give:

$$F_{\mathcal{K},\mathcal{L}} = F_{\mathcal{K},\delta} = -F_{\mathcal{L},\delta} = -m(\delta) K \left(\frac{p_{\mathcal{L}} - p_{\mathcal{K}}}{d_{\mathcal{K},\mathcal{L}}} \right) \tag{21}$$

where K is the harmonic average of the permeabilities in cells κ and $\mathcal{L}$.

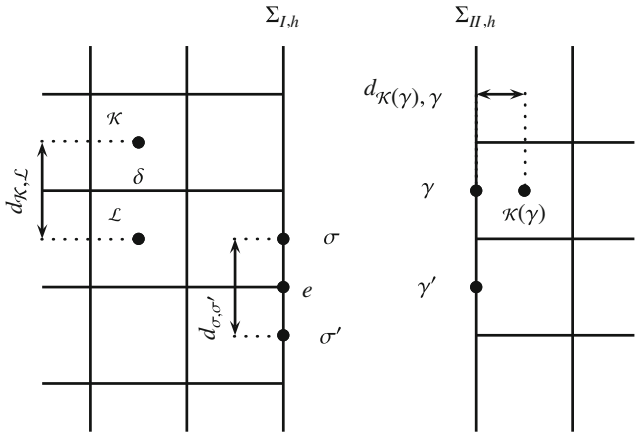

Fig. 5 Discrete notations

The two-point flux approximation on each edge $\int_\sigma \mathbf{v_1}.\mathbf{n}_{|\Sigma}$ denoted by F^1_σ gives:

$$F^1_\sigma = -m(\sigma) K \left(\frac{p^1_\sigma - p^1_{\mathcal{K}(\sigma)}}{d_{\mathcal{K}(\sigma),\sigma}} \right), \ \forall \sigma \in \Sigma_{\mathrm{I},h} \tag{22}$$

where K is the permeability of the cell $\kappa(\sigma)$ connected to the edge σ.

Flow along the fault The finite volume discretisation of the mass balance equation along the fault (Eq. 11) gives:

$$G_\sigma - F^{f,1}_\sigma + \sum_{\substack{e,\\ e \text{ vertex of } \sigma}} G_{\sigma,e} = m(\sigma) \frac{b_f}{2} Q_{f,\sigma}, \quad \forall \sigma \in \Sigma_{\mathrm{I},h} \tag{23}$$

where:

- $Q_{f,\sigma} = \frac{1}{m(\sigma)} \int_\sigma Q_f \mathrm{d}s$.
- $G_{\sigma,e}$ represents the along fault flux across the vertex e out of σ, which approximates $\int_e V_{f,\mathrm{I}}$.
- $F^{f,1}_\sigma$ represents the fault–matrix flux which approximates $\int_\sigma v_{fn,1}$, for $\sigma \in \Sigma_{\mathrm{I},h}$.
- G_σ represents the fault–fault flux which approximates $\int_\sigma v_{fn,\mathrm{I/II}}$ across edge σ.

Figure 6 shows the different discrete fluxes.

For $e = \sigma|\sigma'$, flux conservation and continuity of the pressure give:

$$G_{\sigma,\sigma'} = G_{\sigma,e} = -G_{\sigma',e} = -K_{ft} \frac{b_f}{2} \left(\frac{P^f_{\sigma'} - P^f_\sigma}{d_{\sigma,\sigma'}} \right) \tag{24}$$

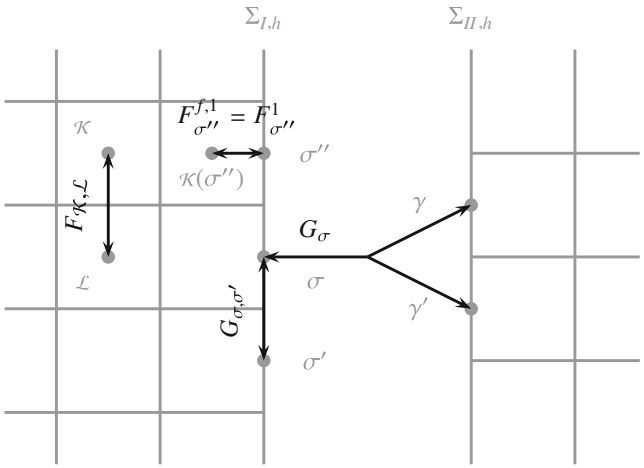

Fig. 6 The different fluxes: matrix flux ($F_{\mathcal{K},\mathcal{L}}$), along the fault flux ($G_{\sigma,\sigma'}$), fault–matrix flux ($F^1_{\sigma''}$), fault–fault flux (G_σ)

For $e \in \partial\Sigma$, the Dirichlet boundary condition leads to:

$$G_{\sigma,e} = -K_{ft}\frac{b_f}{2}\left(\frac{p_f^D(e) - P_\sigma^f}{d_{\sigma,e}}\right) \tag{25}$$

Discretisation of Eq. 15 for the fault–matrix flux gives:

$$F_\sigma^{f,1} = -m(\sigma)\frac{4K_{fn}}{b_f}(P_\sigma^f - p_\sigma^{f,1}), \quad \forall\sigma \in \Sigma_{\mathrm{I},h} \tag{26}$$

The fault–fault flux G_σ across edge σ from side 1 of the fault to side 2 is decomposed into a sum of fluxes across subedges $(\sigma|\gamma)$ that have only one neighbouring edge γ on the other side of the fault (see Fig. 7):

$$G_\sigma = \sum_{\substack{\gamma,\\ \gamma\cap\sigma\neq\emptyset}} G_{\sigma,\gamma} \tag{27}$$

where $G_{\sigma,\gamma}$ denotes an approximation of $\int_{\sigma|\gamma} v_{fn,\mathrm{I/II}}$ and $\sigma|\gamma$ the subedge $\sigma\cap\gamma$.

Approximation of $\int_{\sigma|\gamma} v_{fn,\mathrm{I/II}}$ by the midpoint rule gives:

$$\int_{\sigma|\gamma} v_{fn,\mathrm{I/II}} \simeq m(\sigma|\gamma)v_{fn,\mathrm{I/II}}(e) \tag{28}$$

where e is the center of the subedge $\sigma|\gamma$ and $m(\sigma|\gamma)$ its measure.

Following the finite volume principle of conservation and using Eq. 10, one obtains for $G_{\sigma,\gamma}$:

$$G_{\sigma,\gamma} = -G_{\gamma,\sigma} = -m(\sigma|\gamma)K_{fn}\left(\frac{P_{\gamma|\sigma}^f - P_{\sigma|\gamma}^f}{b_f/2}\right) \tag{29}$$

where $P_{\sigma|\gamma}^f$ (resp. $P_{\gamma|\sigma}^f$) is an approximation of the pressure at the center of the subedge in σ (resp. γ) (see Fig. 7).

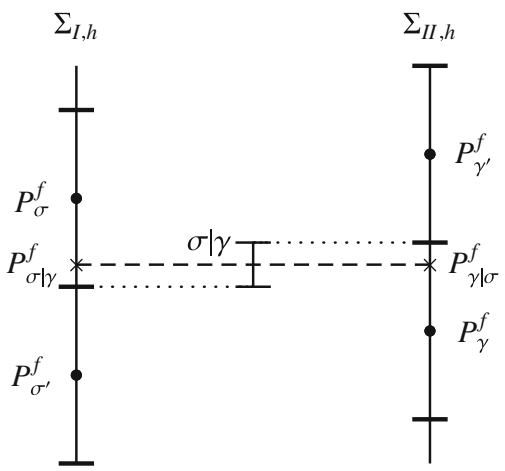

Fig. 7 Fault–fault exchanges

There are several possibilities to compute the pressure $P_{\sigma|\gamma}^f$. The simplest way is to consider a piecewise constant approximation:

$$P_{\sigma|\gamma}^f = P_\sigma^f \tag{30}$$

However, this approximation leads to a non-consistent approximation of $v_{fn,\mathrm{I/II}}(e)$ unless σ and γ are the same edge. It is then necessary to introduce a first-order approximation. This problem is close to the one encountered when discretising diffusion equations on general meshes with cell-centered finite volume which is still a problem studied by many authors. Therefore, we consider only here a very simple approximation, which could in the future take advantages of new advances for diffusive flux approximation.

The simple approximation used here is the following:

$$P_{\sigma|\gamma}^f = \alpha_1 P_\sigma^f + (1-\alpha_1)P_{\sigma'}^f \tag{31}$$

where σ' is the appropriate neighbouring face of σ, as presented in Fig. 7 and α_1 is defined by:

$$\alpha_1 = \frac{(s_{\sigma'} - s_e)}{(s_{\sigma'} - s_\sigma)}$$

where s_σ (resp. $s_{\sigma'}$) is the curvilinear coordinate of σ(resp. σ').

Transmission conditions The transmission conditions between the fault and the matrix (Eq. 19) are written for each fault edge:

$$p_\sigma^{f,1} = p_\sigma^1, \quad F_\sigma^{f,1} = F_\sigma^1, \quad \forall\sigma \in \Sigma_{\mathrm{I},h} \tag{32}$$

Discrete model Using Eqs. 32, 22, 26 and their counterpart on $\Sigma_{\mathrm{II},h}$, it is possible to eliminate the unknowns p_σ^i, $p_\sigma^{f,i}$, $F_\sigma^{f,i}$ for all $\sigma \in \Sigma_{j,h}$, $(i, j) = \{(1, \mathrm{I}), (2, \mathrm{II})\}$. We end up with a discrete model where the main equations are mass balance in each matrix cell and in each fault edge of the two fault sides and the main unknowns are $p_\mathcal{K}$ and P_σ^f. The set of discrete equations forms a linear system which is solved with a standard linear solver (no domain decomposition has been implemented although it could be considered).

2.2 Some results on non-matching grids

Focusing on the non-matching grids problem, this section is dedicated to the validation and the analysis of the model proposed in this paper. Different tests were performed, in which the influence of the fault and matrix properties are studied.

To validate the model, only cartesian grids composed of quadrangles are considered. The throw is constant

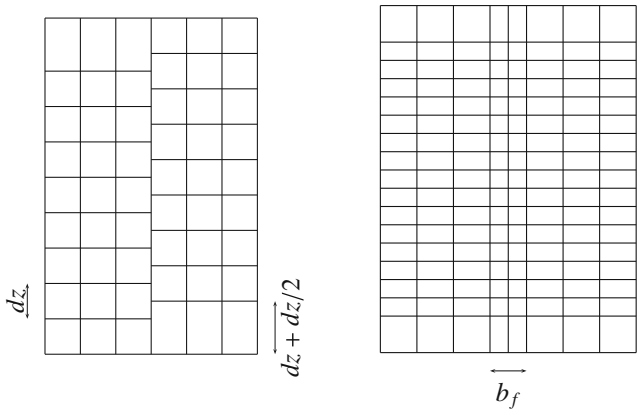

(a) Interface mesh (b) Co-refined reference mesh

Fig. 8 Meshes used

and equal to a half cell height. The matrix is isotropic and the fault homogeneous. To qualify the results obtained with the interface model, we compare them to a so-called reference solution which is computed with the volumetric model on a matching grid. More precisely, this grid is a co-refined mesh of $\Omega_{1,h}$ and $\Omega_{2,h}$ that is to say the coarser common submesh of the two subdomain meshes. It is moreover increased by matching columns of cells that mesh the fault domain Ω_f (see Fig. 8).

We consider here only two columns of cells as it is somehow the best solution one can obtain with the interface model. Indeed, for matching cartesian grid, it has been shown in the literature that the discrete interface model is equivalent to the volumetric one where only one column of cell is used to represent the fault domain [11] and that it gives results that are in good agreement with the converged discrete solution of the volumetric model [20].

We are going to study the influence of the approximation chosen to compute the fault–fault exchange terms, namely we are going to compare the results obtained with Eq. 30 that we call "piecewise constant approximation" to the one obtained with Eq. 31 called "linear approximation". The comparison is performed on the pressure profile along the fault line segment. In the following figures, the pressure profiles along the fault for the interface model ($P_{f,\mathrm{I}}$ and $P_{f,\mathrm{II}}$) are plotted with blue dashed line for the left part of the fault and green dashed line for the right part of the fault. For the reference solution, the pressure profiles ($p_f(-b_f/2, .)$ and $p_f(b_f/2, .)$)) are plotted with black solid line for the left part of the fault and in red solid line for the right one. When the curves for the two sides of the fault are merged, only one curve appears in the figure.

Figure 9a presents the general problem configuration. The domain is $[0, 2] \times [0, 1]$, and the permeability in the matrix is homogeneous, isotropic and such that $K_m = 1$. Three different kinds of faults are considered:

- Permeable fault: $K_f = 100$
- Impermeable fault: $K_f = 0.01$
- Anisotropic fault: $K_{f,t} = 50$, $K_{f,n} = 0.02$

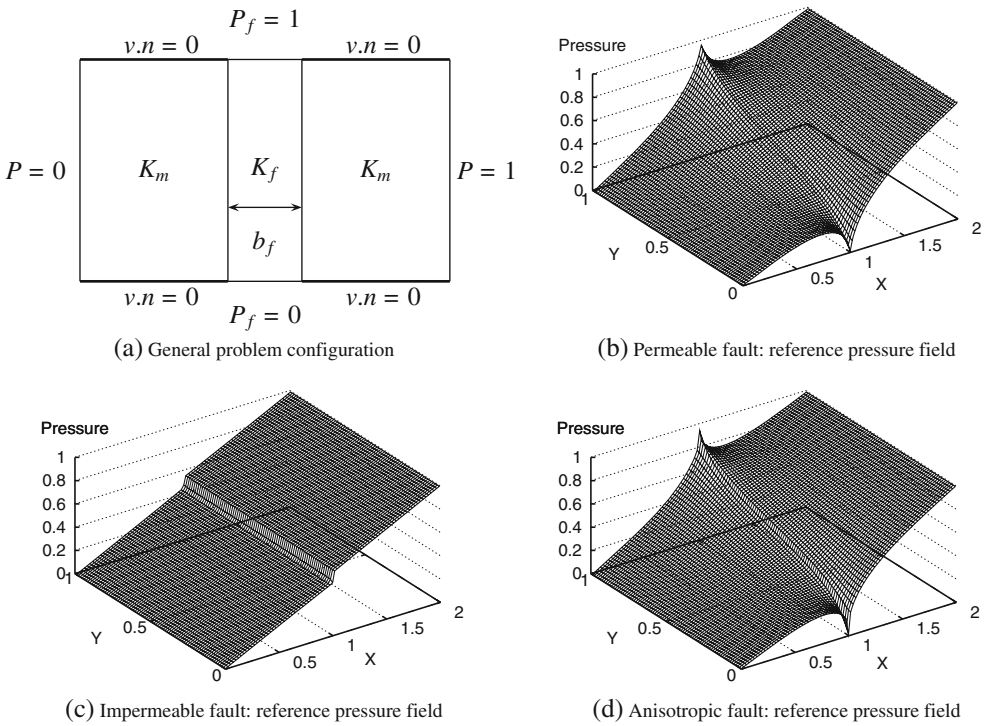

(a) General problem configuration (b) Permeable fault: reference pressure field

(c) Impermeable fault: reference pressure field (d) Anisotropic fault: reference pressure field

Fig. 9 **a** General problem configuration. Reference pressure field for: **b** a permeable fault, **c** an impermeable fault, **d** an anisotropic fault

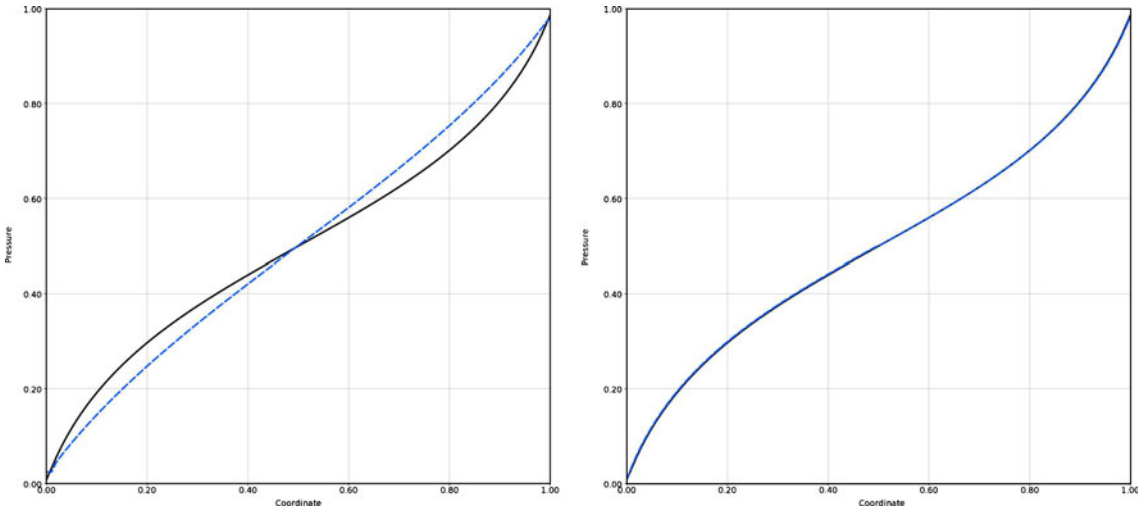

(a) Piecewise constant approximation (b) Linear approximation

Fig. 10 Pressure along the permeable fault. *Black solid* reference solution, *blue dashed* interface solution. The pressure profile is almost the same on both sides of the fault

The fault width is, for these three cases, $b_f = 2 \times 10^{-3}$, and 200 cells are used along the fault for the interface model. Figure 9b–d gives the reference pressure field obtained for the permeable, impermeable and anisotropic fault.

Figure 10 presents the results obtained for the permeable fault for the piecewise constant approximation (Eq. 30) and the linear approximation (Eq. 31) for the fault–fault exchanges.

We first notice that for both approximations (piecewise constant or linear), the pressure is constant through the fault width, as the curves for the two sides of the fault are merged. This is in agreement with the expected behavior as for a permeable fault, the pressure is continuous across the fault. Comparing now the two approximations, it appears that the non-consistency of the piecewise constant approximation gives a poor approximation of the pressure profile along the fault, whereas the linear approximation matches pretty well the reference solution.

Figure 11 presents the pressure profiles along the impermeable fault. Unlike the permeable test case, we

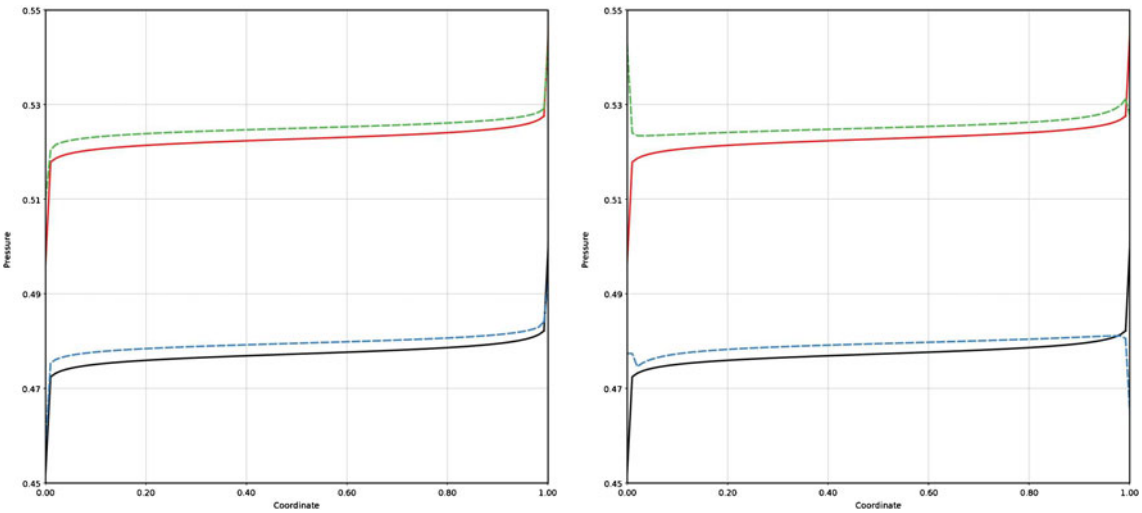

(a) Piecewise constant approximation (b) Linear approximation

Fig. 11 Pressure along the impermeable fault. *Solid lines* reference solution, *dashed lines* interface solution. In each plot, the *lower curves* correspond to the pressure in the *left fault half* while the *upper ones* correspond to its *right half*

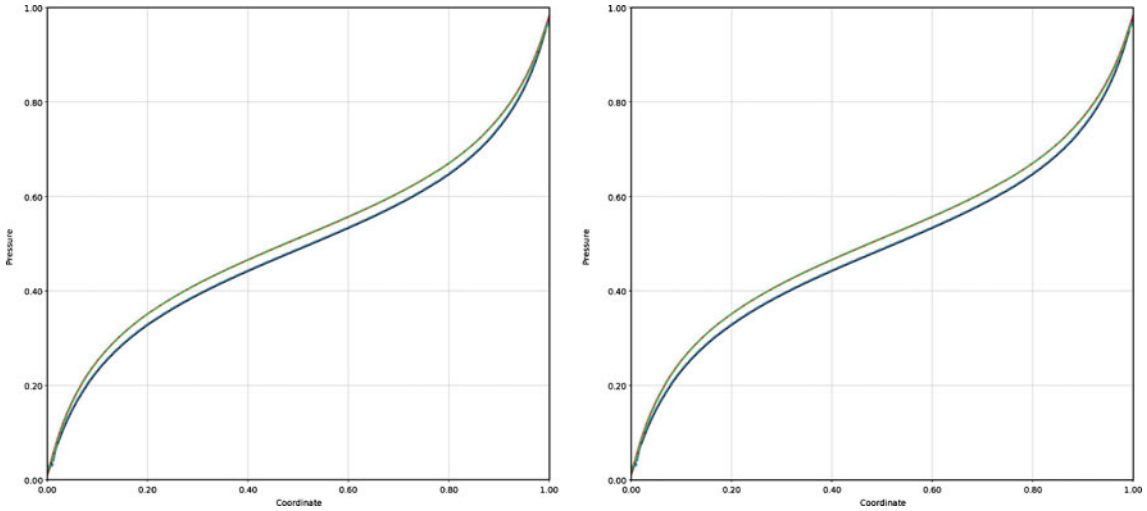

(a) Piecewise constant approximation (b) Linear approximation

Fig. 12 Pressure along the anisotropic fault. *Solid lines* reference solution, *dashed lines* interface solution. Interface and reference solutions are very close

observe that the pressure varies through the fault width. The pressure computed with the piecewise constant approximation is a bit over-evaluated compared to the reference solution. The linear approximation does not give a good result. At the extremities of the fault, the pressure profile exhibits overshoots or undershoots probably linked to the Dirichlet boundary conditions which enforce very strong pressure variations. The linear approximation does not ensure that the maximum principle is respected.

Figure 12 presents the results obtained for the anisotropic fault. We can see that both approximations give a satisfactory solution: The pressure profiles in the two halves of the fault zone are slightly different due to low permeability across the fault and are well captured by the interface model. This is the main difference with the permeable fault: The pressure is not continuous across the fault.

2.2.1 Heterogeneous matrix

This test aims at studying the behavior of the model in a somewhat more realistic configuration from the geological point of view. We consider a domain that includes two geometrically disconnected permeable layers that are linked through a permeable fault (see Fig. 13a).

The considered domain is $[0, 8] \times [0, 8]$. The matrix is heterogeneous and isotropic: $K_1 = 10^{-2}$ and $K_2 = 100$. The fault is isotropic with a large permeability: $K_f = 100$ and a small width: $b_f = 2 \times 10^{-3}$. Homogeneous Neuman boundary conditions hold on the fault extremities. There are 200 cells along the fault for the interface solution.

Figure 13b presents the reference pressure field obtained for this test case, and Fig. 14 presents the results obtained. The numerical solutions exhibit again the behavior encountered in the first test with the permeable

Fig. 13 **a** Problem configuration. **b** Reference pressure field

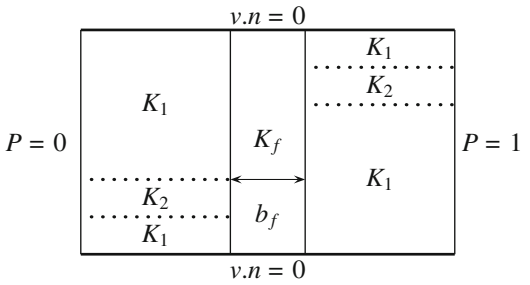

(a) Heterogeneous problem configuration

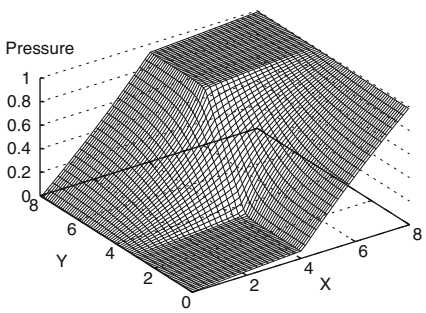

(b) Reference pressure field

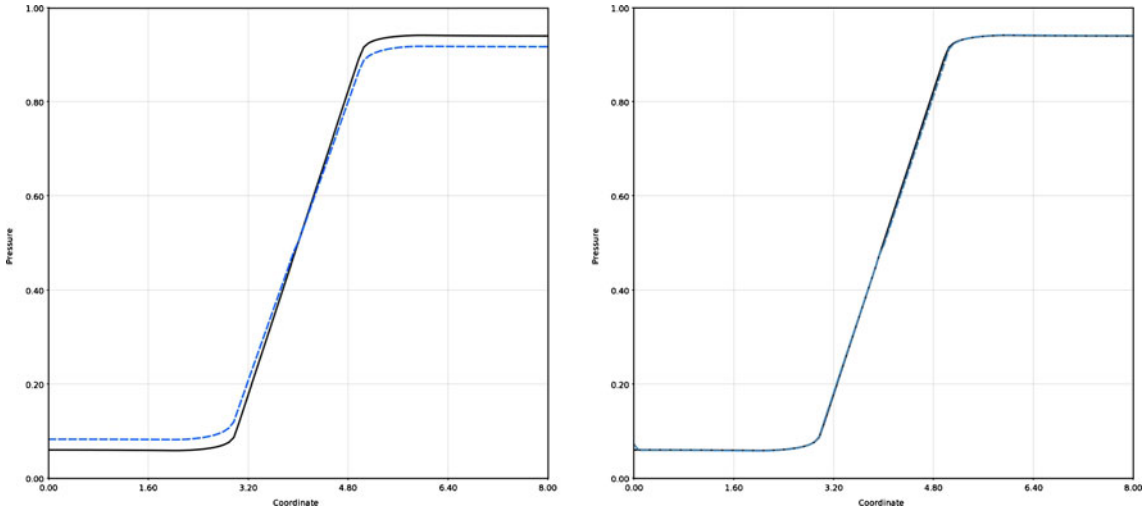

(a) Piecewise constant approximation (b) Linear approximation

Fig. 14 Pressure along the permeable fault in a heterogeneous matrix. *Solid lines* reference solution, *dashed lines* interface solution. The curves of the two sides of the fault are not merged because of the non-matching grid

fault. Indeed, with the piecewise constant approximation, the pressure gradient along the fault is too much dissipated while it is fairly well captured with the linear approximation.

2.3 L-shaped fault

Through an academic problem, this section gives a first insight into a particular difficulty that must be addressed before considering real field faults. Although not properly derived from the volumetric model, we suggest particular numerical approximations to extend the discrete interface fault model. The problem considered is a non-planar fault, which is addressed here in one of its "stiffer" configuration, an "L-shaped" fault, i.e. a fault composed of two orthogonal line segments. The corner of the fault is a particular vertex of the fault grid on both sides of which the normal along the fault is not continuous. In the interface model discretisation, this has to be accounted for in the approximation of the flux along the fault (Eq. 24). We therefore introduce two normals on the vertex e located at the corner of the fault (see Fig. 15), one on each side of the vertex.

In this configuration, the fluxes along the fault, for this vertex e, are given by:

$$G_{\sigma,e} = -K_{ft}\frac{b_f}{2}\left(\frac{p_e - p_\sigma}{d_{\sigma,e}}\right) \tag{33}$$

$$G_{\sigma',e} = -K_{ft}\frac{b_f}{2}\left(\frac{p_e - p_{\sigma'}}{d_{\sigma',e}}\right) \tag{34}$$

To study numerically the proposed approximation, we consider the problem sketched in Fig. 16a, where the domain is $[0, 2] \times [0, 2]$. Dirichlet boundary conditions hold near the two domain corners (0,1) and (1,0) in order to generate a fluid flow across the fault. Two hundred cells along the fault were used for this test. One can see the reference solution on Fig. 16b, computed with the volumetric model for a permeable fault on a matching cartesian grid where the fault domain is represented by two rows of cells.

Figure 17 shows the results obtained for a permeable fault and Fig. 18 for an impermeable one. There is a good agreement between the pressure profiles along the fault of the reference and the interface models. This approach can be extended to a fault with several angles by defining two normals for each vertex considered. Indeed, one normal for each adjacent edge is computed such that it stays inside each edge's plan.

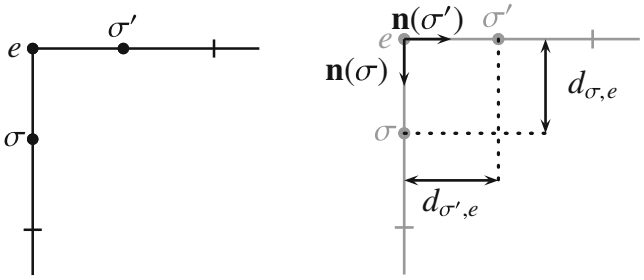

(a) Problem presentation (b) Introducing two normals for vertex e

Fig. 15 Non-planar fault problem

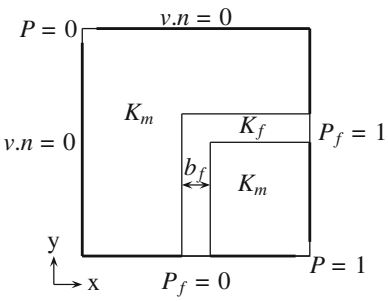

(a) Problem configuration for a L-shaped fault

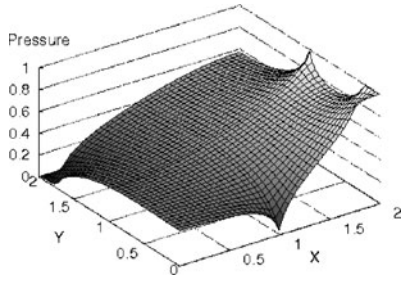

(b) Reference pressure field for a permeable fault

Fig. 16 **a** Problem configuration and **b** reference pressure field

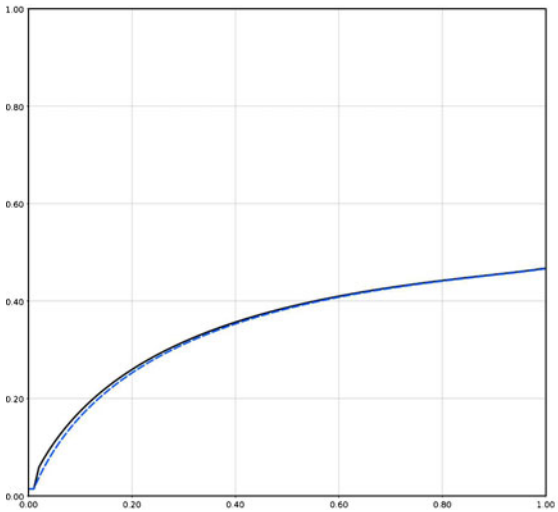

(a) Pressure profile along the x constant part of the fault

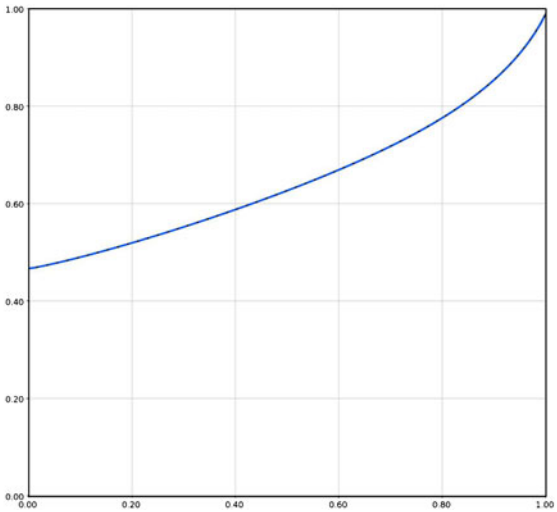

(b) Pressure profile along the y constant part of the fault

Fig. 17 Permeable L-shaped fault. *Black solid line* reference solution, *blue dashed line* interface solution. The curves for the two sides of the fault are merged

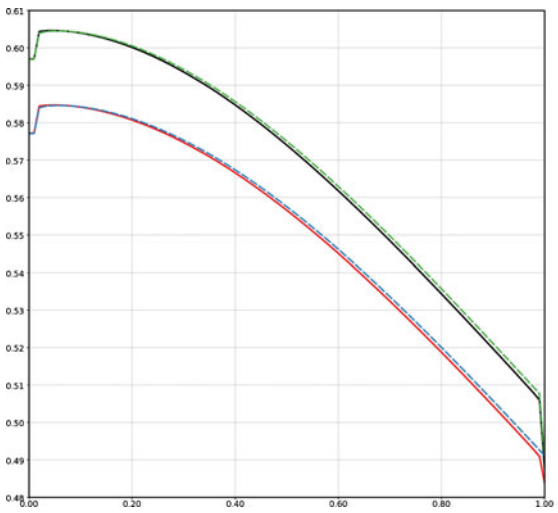

(a) Pressure profile along the x constant part of the fault

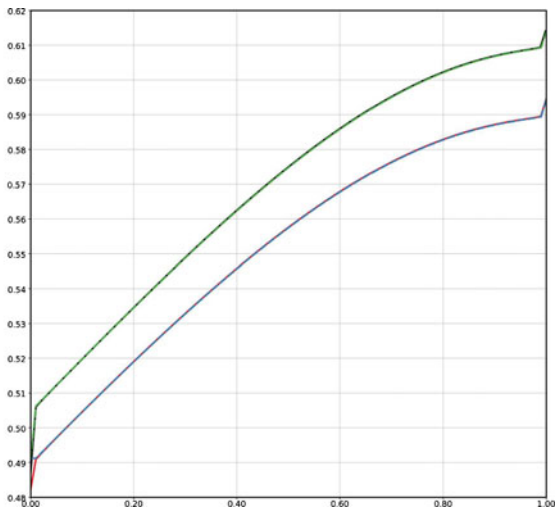

(b) Pressure profile along the y constant part of the fault

Fig. 18 Impermeable L-shaped fault. The *lower curves* correspond to the pressure in the *left half* of the fault while the *upper ones* correspond to its *right half*. *Black and red solid lines* reference solution, *green and blue dashed lines* interface solution

2.4 Discussion

In this section, we have derived an interface fault model and studied its behaviour for a simple academic problem for which a reference solution can be computed. On the discrete point of view, this model is naturally discretised on grids that do not match across faults. The discretisation is based on a cell-centered finite volume scheme combined with a piecewise constant or linear approximation of the pressure for the fault–fault fluxes. Compared to the set of discretised equations classically obtained when considering only flow across faults, this model introduced additional mass balance equations on each fault face, associated to additional pressure unknowns located at fault face centers. The numerical results illustrate the ability of the model to capture the main components of flow along a fault especially when the linear pressure approximation is considered. This study performed in an academic framework confirms the effectiveness of the proposed approach which has now to be extended to more general grids, namely grids that are not orthogonal such as well-known CPG grids. This is the main objective of the next part of this paper.

3 Extension to 3D non-K-orthogonal grids

Following our main goal, which is to propose a model for fluid flow along the faults that can be used in standard oil industry simulators, we make a step forward in considering real case applications. Indeed, we want to extend the proposed approach to 3D non-K-orthogonal grids such as usual CPG grids that are popular in reservoir modeling. Contrary to the first part of the paper, we step directly into the numerical discretisation stage. Our aim is to indicate how classical finite volume discretisations used for flow problems on CPG-type grids can be extended to handle conductive faults through the interface fault model. The most commonly finite volume scheme used in commercial reservoir simulators is probably the two-point scheme. However, this approximation is only valid for K-orthogonal grids. Therefore, we consider here a more accurate approximation, namely the O-scheme (see "Appendix" for a brief presentation of the principle, [1] and references therein for a complete description) although other schemes can be considered such as the two-point scheme or other MPFA approximations. In the following sections, we present the discrete interface model. We then introduce some numerical results on a synthetic test case that mimics a real one.

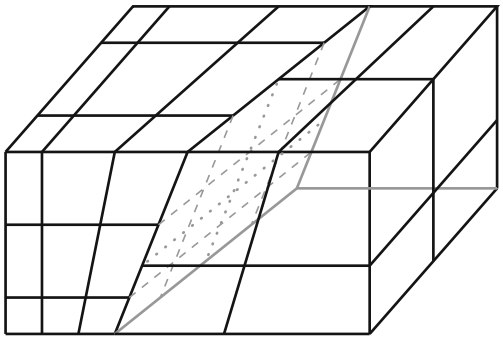

Fig. 19 Schematic 3D grid. Although CPG grids usually share the same pillars, we have represented a grid which is fully non-matching across the fault. Fault faces of the left block are shown in *dashed lines* while fault faces of the right block are in *dotted lines*

3.1 Discrete interface model

We are going to extend the discrete interface model introduced in the first part for 2D cartesian grids and line segment faults to non-planar faults represented as non-matching interfaces in 3D. So let us consider a 3D domain cut by faults, gridded with a mesh that is non-matching across faults, i.e. a fault is represented by two sets of faces, one for each side of the fault (Fig. 19). Following the interface model principle, fluid flow along the fault is modeled by adding discrete pressure unknowns for each face of the fault surfaces which are associated to a corresponding fluid mass balance.

Once again, we present the scheme for one side of the fault (Fig. 20). If we still denote by $\Sigma_{I,h}$ the mesh of the first side of a fault and by σ a face of $\Sigma_{I,h}$, the mass

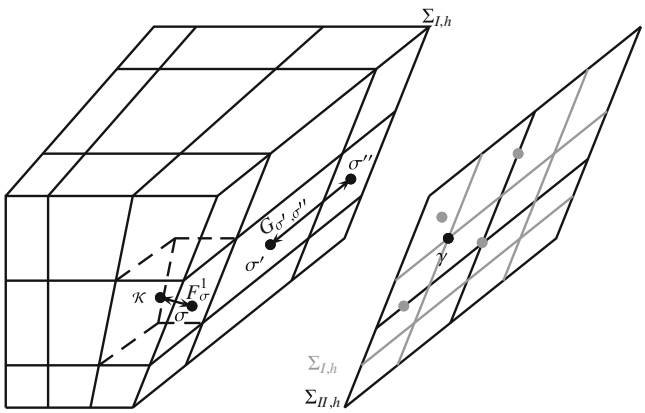

Fig. 20 Fault grid. On the *left*: first part of the fault, flux along the fault ($G_{\sigma',\sigma''}$) and fault–matrix flux (F^1_σ). On the *right*: second part of the fault; the first part of the fault is plotted in *grey line*

balance equation associated to the flow along the first side of the fault writes:

$$G_\sigma - F_\sigma^{f,1} + \sum_{\substack{e,\\ e \text{ edge of } \sigma}} G_{\sigma,e} = m(\sigma)\frac{b_f}{2} Q_{f,\sigma}, \quad \forall \sigma \in \Sigma_{\mathrm{I},h} \tag{35}$$

where:

- $Q_{f,\sigma} = \frac{1}{m(\sigma)} \int_\sigma Q_f \mathrm{d}s$.
- $F_\sigma^{f,1}$ represents the fault–matrix flux which approximates $\int_\sigma v_{fn,1}$, for $\sigma \in \Sigma_{\mathrm{I},h}$, the flux between the fault face σ and its neighbouring matrix cell.
- G_σ represents the fault–fault flux which approximates $\int_\sigma v_{fn,\mathrm{I/II}}$, the flux between the two sides of the fault, across face σ.
- $G_{\sigma,e}$, represents the along the fault flux which approximates $\int_e \mathbf{V}_{\mathbf{f},\mathrm{I}}.\mathbf{n}_{\sigma,e}$, the flux along the fault surface, across the edge e, out of σ.

For this last term, an additional difficulty occurs as the fault surface is not necessarily planar.

Therefore, for each edge e of $\Sigma_{\mathrm{I},h}$, we introduce two normals, one for each of its adjacent faces. Let $\mathbf{n}_\sigma$ be the normal to the face σ oriented in an arbitrary way; $\mathbf{n}_{e,\sigma}$ is the unit vector simultaneously orthogonal to the edge e and to $\mathbf{n}_\sigma$ oriented outside of σ (Fig. 21). If the face is not planar, we take $\mathbf{n}_\sigma$ as the average normal of the face.

Before going into details, let us give an overview of the approach chosen to approximate the different fluxes. Although not detailed in the following, the mass balance equations in the matrix are classically discretised using the O-scheme. For the fault, we are going to use the O-scheme to compute the along fault fluxes $G_{\sigma,e}$ across the edges e of the fault surfacic mesh. Then, for the flux G_σ between the two fault sides, we generalize the linear approximation introduced in the first part of this paper, by taking advantage of the along fault pressure gradient approximation associated to the O-scheme. Finally, the flux between a fault face and its adjacent matrix cell combines the O-scheme flux approximation on the matrix side with Eqs. 15 or 16. In the next paragraphs, we first describe the computation of the fluxes $G_{\sigma,e}$ and G_σ, and then we precise how the flux $F_\sigma^{f,1}$ is approximated.

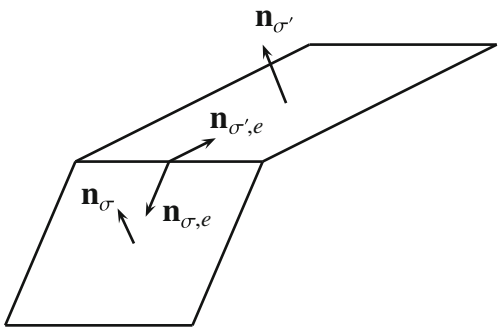

Fig. 21 Introduction of two normals for each edge e of $\Sigma_{\mathrm{I},h}$

Along the fault fluxes We want to compute $G_{\sigma,e}$, an approximation of $\int_e \mathbf{V}_{\mathbf{f},\mathrm{I}}.\mathbf{n}_{e,\sigma}$, across the edge e, out of σ where $\mathbf{V}_{\mathbf{f},\mathrm{I}}$ is given by Eq. 13. The O-scheme principle recalled in "Appendix" can be straightforwardly applied considering the surfacic mesh $\Sigma_{\mathrm{I},h}$. Indeed, the gradient approximation given by the O-scheme holds here. The flux $G_{\sigma,e}$ is then given by:

$$G_{\sigma,e} = \sum_{\substack{\gamma,\\ \gamma \text{ neighbours of } \sigma}} b_{\sigma,\gamma} P_\gamma^f \tag{36}$$

The neighbouring faces of σ are all the faces γ that share a vertex with σ. The coefficient $b_{\sigma,\gamma}$ is given by the O-scheme (see "Appendix").

Fault–fault flow As for the line segment fault, the flux G_σ is decomposed into a sum of fluxes across subfaces $(\sigma|\gamma)$ that have only one neighbouring face γ on the other side of the fault (Fig. 20).

Then $G_\sigma = \sum_{\substack{\gamma \in \Sigma_{\mathrm{II},h} \\ \gamma \cap \sigma \neq \emptyset}} G_{\sigma,\gamma}$ where $G_{\sigma,\gamma}$ is still defined by:

$$G_{\sigma,\gamma} = -m(\sigma|\gamma) K_{fn} \left(\frac{P^f_{\sigma|\gamma} - P^f_{\gamma|\sigma}}{b_f/2} \right) \tag{37}$$

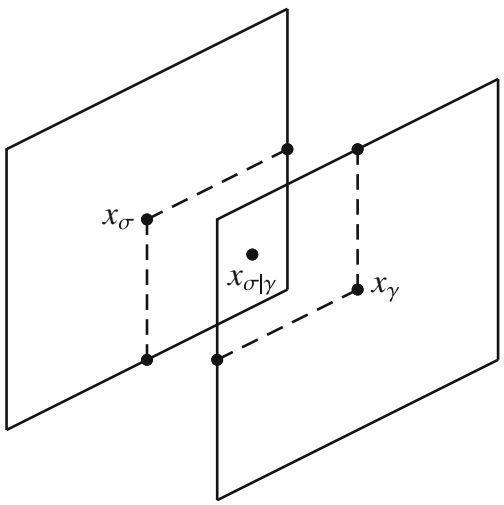

Fig. 22 Selection of the interaction volumes for the gradient reconstruction. The interaction volumes for the faces σ and γ are drawn in *dashed lines*

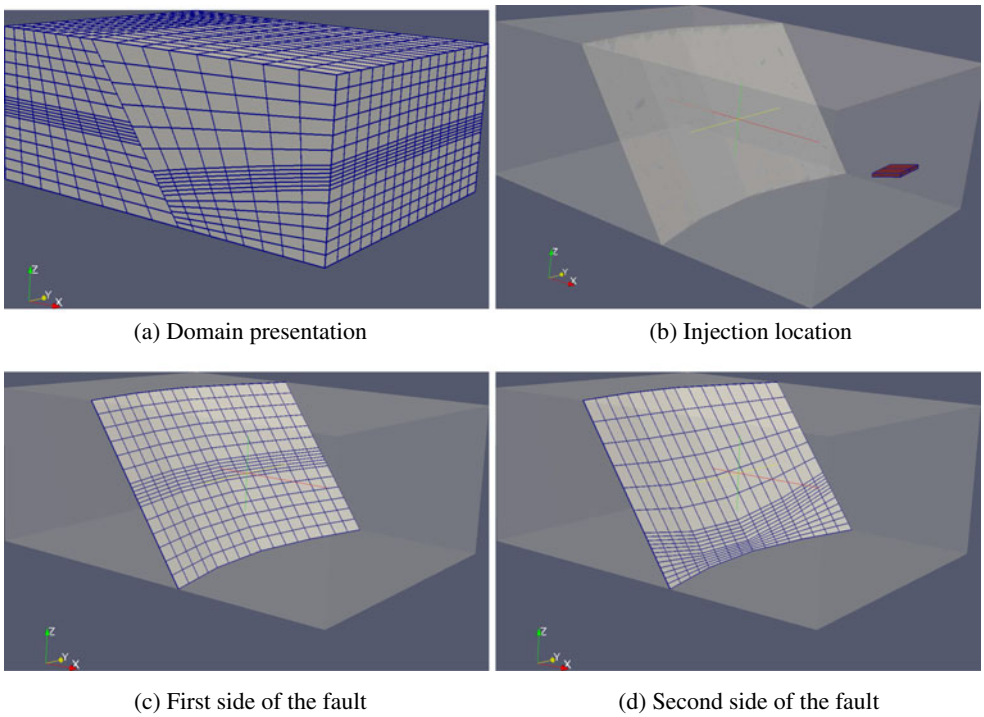

(a) Domain presentation (b) Injection location

(c) First side of the fault (d) Second side of the fault

Fig. 23 Geometry of the synthetic test case

with $P^f_{\sigma|\gamma}$ (resp. $P^f_{\gamma|\sigma}$) an approximation of the pressure at the center of the subface in σ (resp. γ). To perform this approximation, we take advantage of the discrete pressure gradient given by the O-scheme (39), which expresses the pressure gradient in the subregion of the face located in the interaction volume as a linear combination of the pressure unknowns inside the whole interaction volume.

Let us denote by $x_{\sigma|\gamma}$ the center of the subface $\sigma|\gamma$. Among the different interaction volumes that cut σ, we select the one to which $x_{\sigma|\gamma}$ belongs as shown on Fig. 22. If $x_{\sigma|\gamma}$ happens to be on the line segment between two interaction volumes, we simply chose one of them although it could be interesting to perform an average of the two approximations.

The pressure $P^f_{\sigma|\gamma}$ is then given by:

$$P^f_{\sigma|\gamma} = P^f_\sigma + \nabla_{V\cap\sigma} \quad P^f_\sigma.(x_{\sigma|\gamma} - x_\sigma)$$

where x_σ is the center of the faces σ and $\nabla_{V\cap\sigma}$ is the pressure gradient inside the intersection of the relevant interaction volume and the face σ.

Fault–matrix flow The fluxes $F^{f,1}_\sigma$ are approximated simultaneously with the matrix–fault fluxes $\int_\sigma \mathbf{v_1}.\mathbf{n}_{|\Sigma}$, seen from the matrix side. The O-scheme principle is again applied by considering a particular 3D interaction volume around each vertex of the fault surface that is composed of the matrix cells that share that vertex. In this interaction volume, a linear approximation of the pressure is performed in each matrix cell as a function of the cell center pressure and matrix face center unknowns, while Eq. 15 is used to express the flux on the fault faces from the fault side. The usual process leads to fluxes on matrix–fault faces and matrix faces adjacent to the fault, as a linear combination of matrix pressure and fault pressure unknowns.

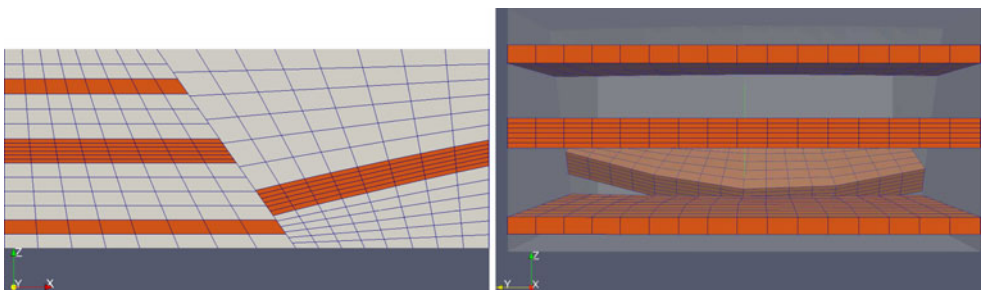

(a) View direction set to $-Y$ (b) View direction set to $+X$

Fig. 24 Domain configuration

Table 1 Domain properties

	Orange cells	White cells	Fault
Porosity (%)	20	1	
Permeability (mD)	$\begin{bmatrix} 100 & 0 & 0 \\ 0 & 100 & 0 \\ 0 & 0 & 10 \end{bmatrix}$	$\begin{bmatrix} 0.1 & 0 & 0 \\ 0 & 0.1 & 0 \\ 0 & 0 & 0.01 \end{bmatrix}$	$\begin{bmatrix} 1{,}000 & 0 & 0 \\ 0 & 1{,}000 & 0 \\ 0 & 0 & 1{,}000 \end{bmatrix}$
Compressibility (bar^{-1})	10^{-4}	10^{-4}	0

3.2 Realistic test case

In this section, the fault model proposed in this paper is tested on a synthetic test which mimics a real test configuration, inspired by CO_2 storage problem. The following equation is solved:

$$\phi c \frac{\partial p}{\partial t} - \nabla \cdot \left(\frac{\mathbf{K_m}}{\mu} \nabla p\right) = q \tag{38}$$

where ϕ is the porosity, $\mathbf{K_m}$ the matrix's permeability tensor, c is the compressibility, μ the fluid viscosity and q is the source term that corresponds to an injection well. In the interface fault model, the accumulation term is neglected as the fault width is small. It could, however, have been kept.

Test case configuration The meshed domain is presented in Fig. 23a. The two parts of the fault are presented in Fig. 23c, d. The domain is approximatively 6,000 m in the x direction, 4,800 m in the y and 2,450 m in the z direction. The fault's width is constant and equal to 5 m.

An injection of 10 m^3/day is performed for 30 years in the cells showed in Fig. 23b. On the opposite vertical boundary, a pressure of 0 Pa is imposed on all the faces during the simulation. Everywhere else, no-flow boundary conditions hold. The fluid viscosity is $\mu = 1$ cP. The fault connects one permeable layer on the right side to three other permeable ones on the left side (in orange on Fig. 24a). Without a model for fluid flow along the faults, these permeable layers would not have been connected. The parameters used are summarized in Table 1, the different layers can be seen in Fig. 24a and the connection between two permeable layers is observable in Fig. 24b.

Simulation results As there is no reference solution for this test, the results are analysed in a qualitative manner. Two simulations have been performed to study the impact of the approximation chosen for the flow along and across the fault. For the two of them, the O-scheme is used to compute the fluxes in the matrix. For the fluxes associated to the fault, the two-point and O-scheme described above are compared. For the sake of simplicity, we have, however, always used a two-point scheme for the flux on outside boundary faces. In the following, the pressure is given in Pascal.

Figure 25a, b presents the pressure in the matrix after 9 months of injection for the two-point and the O-scheme (the pressure scale has been rescaled to enhance the readability). One can see that the pressure inside the three permeable layers after the fault is high, compared to the injection point, even if two of them are not connected to the injection layer. This implies that the fluids flow from the permeable layer into the fault, then flow along the fault and, finally, to these permeable layers. This illustrates the ability of the approach to account for fluid flow along the fault.

To compare the two approximations, we have plotted on Fig. 26 the evolution of pressure versus time in three matrix's cells located near the fault surface and shown in Fig. 26a. The results obtained with the two-point scheme are drawn in solid red lines, whereas the results obtained with the O-scheme are drawn in black dashed lines.

Figure 27a, b gives the pressure field in the fault after 3 months and after 60 years at the end of the

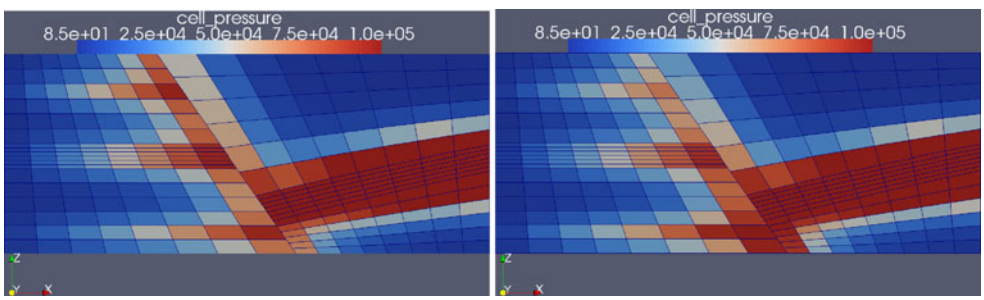

Fig. 25 Pressure in the matrix after 9 months

(a) Two-point scheme (b) O-scheme

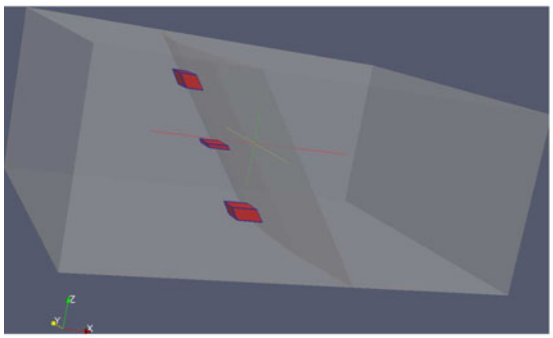

(a) Selected cells

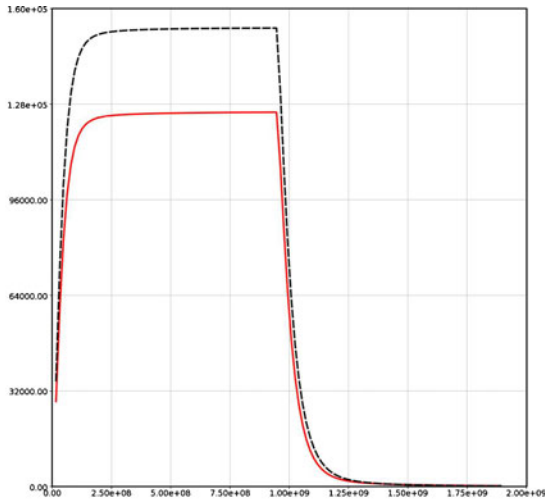

(b) Pressure over the time in the matrix for the bottom cell. Red: two-point scheme, black: O–scheme

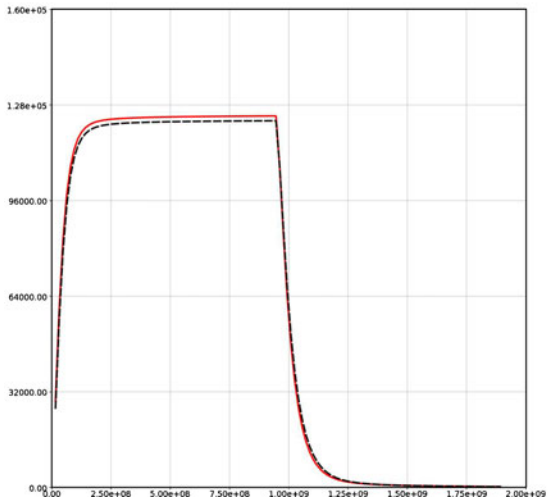

(c) Pressure over the time in the matrix for the middle cell. Red: two-point scheme, black: O–scheme

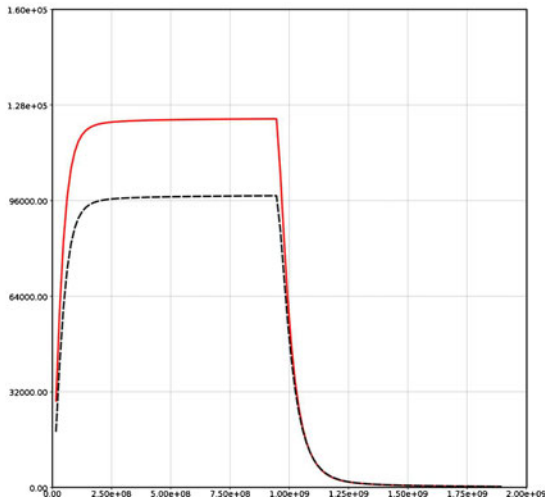

(d) Pressure over the time in the matrix forthe top cell. Red: two-point scheme, black: O–scheme

Fig. 26 **a** Selected cells. **b–d** Pressure over the time in the selected cells

simulation, for the two-point scheme while results for the O-scheme are shown on Fig. 28a, b. The impact of the scheme used is clearly observable, both in the matrix and in the fault. In Fig. 26b, one can see that the pressure calculated using the two-point scheme is underestimated compared to the one found with the

Fig. 27 Results obtained for the two-point scheme

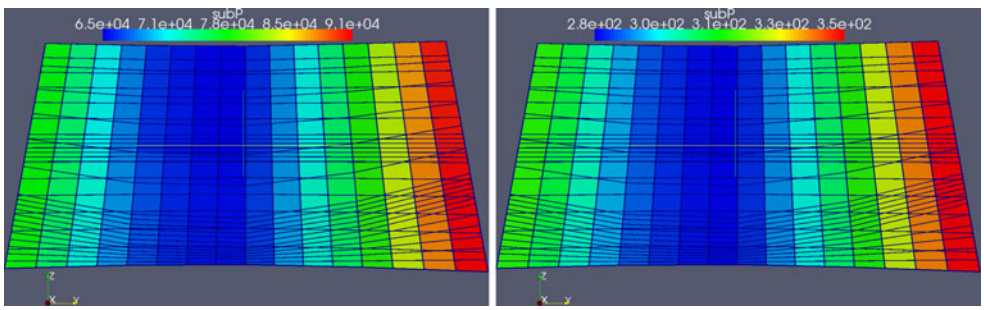

(a) Pressure in the fault after 3 months

(b) Pressure in the fault after 60 years

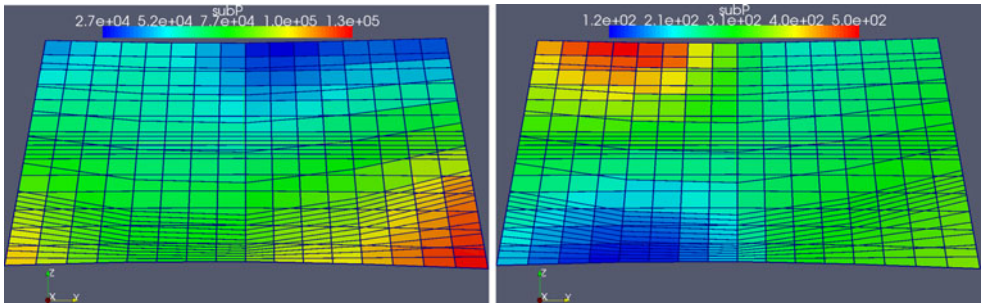

Fig. 28 Results obtained for the O-scheme

(a) Pressure in the fault after 3 months (b) Pressure in the fault after 60 years

O-scheme. At this point, two permeable layers are connected via the fault as shown in Fig. 24b and the two-point scheme does not capture the impact of this connection, as it can be seen in the fault pressure profile. In Fig. 26c, d, one can observe that the pressure is overestimated by the two-point scheme. Concerning the pressure field in the fault depicted in Figs. 27a to 28b, if the scale is almost the same for the two schemes, the profile is completely different. The O-scheme respects the geometry and the connection of the layers via the fault when it calculates the pressure. As it has been seen for the academic problems, the two-point scheme approximation has a tendency to smooth the pressure inside the fault.

4 Conclusion

In this study, an interface model for a single-phase fluid flow in porous media has been proposed. Compared to previous interface fault models found in the literature, the proposed approach considers that the fault is represented by two interfaces instead of one. This enable to handle quite naturally grids that are not matching across the fault, such as the well-known CPG grids. Moreover, this model does not require to introduce new grid elements and add no other difficulties compared to the ones involved when computing fluxes across the fault.

Within a classical finite volume discretisation, the non-matching grids lead to so-called fault–fault fluxes across faces that do not match. Mainly two approximations have been considered, and the first one is based on a piecewise constant approximation of the pressure which is easy and robust but not always accurate enough. Therefore, another approximation based on a piecewise linear approximation has been studied. We have chosen to base this approximation on the O-scheme, but other schemes could have been considered. Although only results with homogeneous faults have been presented, heterogeneous faults can be considered by assigning a different fault permeability tensor to each fault face. Compared to the discrete model classically obtained when accounting only for flow across faults, the proposed model adds unknowns, and corresponding mass balance equations on fault faces, it therefore integrates itself naturally in a simulator based on a general connection-list representation of the grid system.

The model can be extended in several directions. It can for instance be applied in the framework of basin modeling where non-matching evolving grids are considered to follow blocks sliding along faults. Moreover, its extension to a multi-phase flow should be straightforward, as it enters in the finite volume framework. However, we have handled here the problem of very different space scales between the matrix and the fault but problems associated to different time scales remain especially when solving the non-linear system of discrete equations that govern multiphase fluid flow.

Acknowledgements The authors would like to thank two anonymous reviewers for their precious remarks and Laurent Trenty, from IFP Energies Nouvelles, who has provided us the grid for the synthetic test case and for all the useful discussions we had.

Appendix: O-scheme principle

The O-scheme is a cell-centered finite volume scheme that gives an approximation of conductive fluxes on non-K-orthogonal grids. Its principle is briefly recalled here in a 2D framework to avoid cumbersome notations, but the same ideas apply for 3D grids.

Let us consider a 2D grid and a conductive operator $(-\nabla \cdot \mathbf{K}\nabla u)$. Following the finite volume principle, we are led to the approximation of the flux across each edge $\delta : \int_\delta -\mathbf{K}\nabla u.\mathbf{n}$. The first stage of the approximation is to decompose the flux across δ into two fluxes across each half edge associated to one of its vertices. This half flux is then computed using a piecewise linear interpolation of the unknown u around the associated

Fig. 29 Notations for the O-scheme

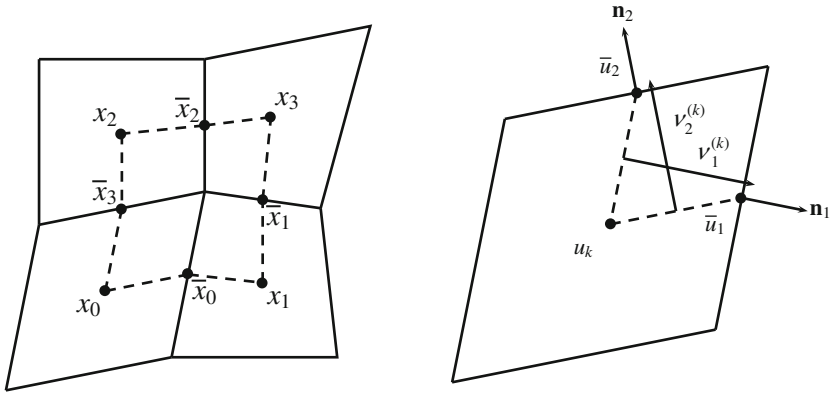

(a) Interaction Volume, composed of 4 subregions, one in each neighbouring cell

(b) Normal vectors for a cell

vertex in a so-called interaction volume (Fig. 29a). For the sake of simplicity, we consider only quadrilateral faces but triangular faces can also be considered. The cell centers are denoted by x_k and the edges midpoints by $\overline{x}_k$. The area determined by these eight points is the interaction volume and is represented in dashed line in Fig. 29a. The piecewise linear approximation is obtained assuming a linear variation of the pressure in each cell and pressure and flux continuity at each point $\overline{x}_k$.

For a cell k in the interaction volume, we denote by u_k the unknown at the cell center, and we introduce two auxiliary unknowns at edge mid-points $\overline{u}_1$ and $\overline{u}_2$ (Fig. 29b). The gradient of the unknown in this cell can be written:

$$\nabla u = \frac{1}{2A_k}[\nu_1^{(k)}(\overline{u}_1 - u_k) + \nu_2^{(k)}(\overline{u}_2 - u_k)] \tag{39}$$

where A_k represents the area of the triangle $x_k\overline{x}_1\overline{x}_2$ and $\nu_1^{(k)}$ and $\nu_2^{(k)}$ the normal vectors of the interaction volume within cell k. The norm of vector $\nu_i^{(k)}$ is equal to Γ_i, the length of the half edge to which it is normal.

Hence, the fluxes through the half edges are given by:

$$\begin{bmatrix} f_1^{(k)} \\ f_2^{(k)} \end{bmatrix} = -\mathbf{B_k} \begin{bmatrix} \overline{u}_1 - u_k \\ \overline{u}_2 - u_k \end{bmatrix} \tag{40}$$

where $f_i^{(k)}$ is the flux through the half edge i of the cell k and $\mathbf{B_k}$ is the matrix defined by:

$$\mathbf{B_k} = \frac{1}{2A_k} \begin{bmatrix} \Gamma_1 \mathbf{n}_1^T \mathbf{K}_k \nu_1^{(k)} & \Gamma_1 \mathbf{n}_1^T \mathbf{K}_k \nu_2^{(k)} \\ \Gamma_2 \mathbf{n}_2^T \mathbf{K}_k \nu_1^{(k)} & \Gamma_2 \mathbf{n}_2^T \mathbf{K}_k \nu_2^{(k)} \end{bmatrix} \tag{41}$$

where $\mathbf{n}_i^T$ is the half edge i unit normal.

Computing the fluxes for all the half edges of an interaction volume and requiring continuity for the fluxes and for the unknown at the midpoints of each edge, it is possible to eliminate the auxiliary unknowns located at the midpoints of the edges. It ends up with a scheme where the fluxes through all half edges are expressed as a linear combination of the cell center unknowns. Finally, the O-scheme provides an expression for the fluxes across each edge as a linear combination of the unknowns in the neighbouring cells, i.e. cells that share a vertex with δ:

$$\int_\delta -\mathbf{K}\nabla u.\mathbf{n} \simeq \sum_{\substack{k, \\ k \text{ neighbour of } \delta}} b_{\delta,k} u_k$$

where $b_{\delta,k}$ is the relevant term of the matrix $\mathbf{B_k}$ defined by Eq. 41.

Replacing unknowns $\overline{u}_1$ and $\overline{u}_2$ in Eq. 39 with their corresponding expressions, the unknown gradient in each sub-region is expressed as a linear combination of cells unknowns:

$$\nabla u = \sum_{l=1}^{4} \mathbf{V}_l u_l$$

where V_l is in $\mathbb{R}^2$. More details can be found in [1].

References

1. Aavatsmark, I.: An introduction to multipoint flux approximations for quadrilateral grids. Comput. Geosci **6**, 405–432 (2002)
2. Alboin, C., Jaffre, J., Roberts, J., Serres, C.: Domain decomposition for flow in porous media with fractures. In: Lai, C.H., Bjorstad, P.E., Cross, M., Widlund, O.B. (eds.) Domain Decomposition Methods in Sciences and Engineering, pp. 365–373. Domain Decomposition, Bergen (1999)

3. Alboin, C., Jaffré, J., Roberts, J.E., Wang, X., Serres, C.: Domain decomposition for some transmission problems in flow in porous media. In: Numerical Treatment of Multiphase Flows in Porous Media, vol. 552, pp. 22–34. Springer, Berlin (2000)
4. Angot, P.: A model of fracture for elliptic problems with flux and solution jumps. C. R. Math. **337**(6), 425–430 (2003)
5. Angot, P., Boyer, F., Hubert, F.: Numerical modelling of flow in fractured porous media. In: Finite Volume for Complex Applications IV, pp. 249–260. Hermes, Paris (2005)
6. Angot, P., Boyer, F., Hubert, F.: Asymptotic and numerical modelling of flows in fractured porous media. Modél. Math. Anal. Numér **43**(2), 239–275 (2009)
7. Arbogast, T., Cowsar, L.C., Wheeler, M.F., Yotov, I.: Mixed finite element methods on nonmatching multiblock grids. Siam J. Numer. Anal. **37**(4), 1295–1315 (2000)
8. Eymard, R., Gallouët, T., Herbin, R.: Finite volume methods. In: Ciarlet, P.G., Lions, J.L. (eds.) Handbook of Numerical Analysis, vol. 7, pp. 713–1020. North-Holland, Amsterdam (2000)
9. Faille, I., Flauraud, E., Nataf, F., Pégaz-Fiornet, S., Schneider, F., Willien, F.: A new fault model in geological basin modelling. application of finite volume scheme and domain decomposition methods. In: Herbin, R., Kröner, D. (eds.) Finite Volume for Complex Applications III: Problems and Perspectives, pp. 543–550. Hermes Penton Science, London (2002)
10. Faille, I., Nataf, F., Saas, L., Willien, F.: Finite volume methods on non-matching grids with arbitrary interface conditions and highly heterogeneous media. In: Kornhuber, R., Hoppe, R., Périaux, J., Pironneau, O., Widlund, O., Xu, J. (eds.) Domain Decomposition Methods in Science and Engineering. Lecture Notes in Computational Science and Engineering, vol. 40 (2004)
11. Flauraud, E.: Méthodes de décomposition de domaine pour les écoulements en milieux poreux. Ph.D. thesis, Université pierre et marie curie, Paris (2004)
12. Flauraud, E., Nataf, F., Faille, I., Masson, R.: Domain decomposition for an asymptotic geological fault modeling. C R Mécanique **331**(12), 849–855 (2003)
13. Fredman, N., Tveranger, J., Cardozo, N., Braathen, A., Soleng, H., Rœ, P., Skorstad, A., Syversveen, A.: Fault facies modeling: technique and approach for 3-d conditioning and modeling of faulted grids. AAPG Bull. **92**(11), 1457–1478 (2008)
14. Frih, N., Roberts, J.E., Saada, A.: Modeling fractures as interfaces: a model for Forchheimer fractures. Comput. Geosci. **12**(1), 91–104 (2008)
15. Gilman, J.R., Bowzer, J.L., Rothkopf, B.W.: Application of short-radius horizontal boreholes in the naturally fractured Yates field. SPE Reserv. Eng. **10**(1), 10–15 (1995)
16. Hearn, C.L., Al-Emadi, I. A.A., Worley, P.L.H., Taylor, R.D.: Improved oil recovery in a tight reservoir with conductive faults, ISND Shuaiba, Qatar. In: SPE Annual Technical Conference and Exhibition. San Antonio, Texas, 5–8 October 1997
17. Karimi-Fard, M., Durlofsky, L.J., Aziz, K.: An efficient discrete-fracture model applicable for general-purpose reservoir simulators. SPE J. **9**(2), 227–236 (2004)
18. Lee, S.H., Jensen, C.L., Lough, M.F.: An efficient finite difference model for flow in a reservoir with multiple length-scale fractures. SPE J. **5**(3), 268–275 (2000)
19. Manzocchi, T., Walsh, J., Nell, P., Yielding, G.: Fault transmissibility multipliers for flow simulation models. Pet. Geosci. **5**(1), 53–63 (1999)
20. Martin, V., Jaffré, J., Roberts, J.E.: Modeling fractures and barriers as interfaces for flow in porous media. Soc Ind Appl Math J **26**(5), 1667–1691 (2005)
21. Ponting, D.K.: Corner point geometry in reservoir simulation. In: 1st European Conference on the Mathematics of Oil Recovery, pp. 45–65. Oxford (1989)
22. Reinchenberger, V., Jakobs, H., Bastian, P., Helmig, R.: A mixed-dimensional finite volume method for two-phase flow in fractured porous media. In: Advances in Water Resources, vol. 29, pp. 1020–1036. Elsevier Science, Oxford (2005)
23. Trocchio, J.T.: Investigation of Fateh Mishrif fluid-conductive faults. J. Pet. Technol. **51**(8), 1038–1045 (1990)
24. Yielding, G., Freeman, B., Needham, T.D.: Quantitative fault seal prediction. AAPG Bull. **81**(6), 897–917 (1997)